Journal of Magnetism and Magnetic Materials 341 (2013) 86–92

Contents lists available at SciVerse ScienceDirect

Journal of Magnetism and Magnetic Materials

journal homepage: www.elsevier.com/locate/jmmm

Breaking of chiral symmetry in vortex domain wall propagation in ferromagnetic nanotubes

J.A. Otálora [a,*], J.A. López-López [a], P. Landeros [a], P. Vargas [a], A.S. Núñez [b]

[a] Departamento de Física, Universidad Técnica Federico Santa María, Avenida España 1680, Valparaíso, Chile
[b] Departamento de Física, Facultad de Ciencias Físicas y Matemáticas, Universidad de Chile, Blanco Encalada 2008, Santiago, Chile

ARTICLE INFO

Article history:
Received 14 November 2012
Received in revised form
27 March 2013
Available online 13 April 2013

Keywords:
Dynamic
Vortex domain wall
Chirality
Magnetic nanotube

ABSTRACT

This paper is focused to the field-induced dynamics of vortex-like domain walls (VDWs) in magnetic nanotubes (MNTs). Based on a dissipative Lagrangian formalism that fully includes damping as well as exchange and dipole–dipole coupling, it is shown that VDW motion is very sensitive to the chirality, giving rise to a chiral asymmetry in the vortex wall propagation. As a consequence, the dynamics of the wall is fundamentally different to that of nanostripes and solid nanowires. Besides the well-known Walker breakdown that stands at the onset of the precessional wall motion, it is found an additional breakdown field (called here the chiral breakdown) that modifies the steady regime of VDWs. We also show outstanding VDWs dynamical properties at low applied fields, as low-field mobilities (~10 km/(sT)) and very short relaxation times (~1 ns), offering a reliable fast control of VDWs velocities (~1000 m/s at applied fields of 0.7 mT).

1. Introduction

The development of newer, faster, and more robust devices based on magnetic nanostructures relies on the knowledge of the properties of its magnetic textures. As examples of potential applications, we find magnetic memories [1], logic devices [2], microwave nano-oscillators [3] and spintronic-based devices [4,5]. The potential to manipulate these devices grows with the advanced synthesis and characterization techniques being developed for nanosystems [6]. For example, over many years there have been extensive investigations about the static and dynamic properties of magnetic domain walls (DWs) in nanostripes and nanowires [7–15]. In fact, it has been argued recently that the control of magnetic DWs may open the way to a new and faster device, the magnetic racetrack memory [1].

The potential technological developments based on DW dynamics have fueled further research about its detailed motion, which can be driven either by electric currents or magnetic fields. Most of the investigations have been focused on nanostripes, where micromagnetic simulations and experimental results have shown that DWs move mainly in two possible regimes: (i) a viscous or steady motion in which the propagation is performed with constant velocity, and (ii) a turbulent or precessional motion wherein the walls propagate suffering oscillations as well as periodic topological transformations in its internal magnetic microstructure [7,9,11,12,14]. Both regimes are separated by the well-known Walker breakdown which defines the Walker magnetic field, if the external excitation is a magnetic field, or the Walker electric current, if the driving force is the spin-transfer from the current to the local magnetic moments. Besides the enormous efforts to describe the DW dynamics deterministically in nanostripes, its topological transformations during the precessional regime involve an important limitation from an analytical point of view, for example, in the evaluation of the strongly non-uniform dipole fields. Because of such complex transformations, the turbulent dynamics is mostly investigated through micromagnetic simulations. Although the simulations offer good insights into the related physics, the turbulent dynamics is still far from being completely understood. This is an important limitation and thus, a complete analytical description of the DW dynamics could allows us to unveil most of the physical details, and very probably new properties, which ultimately define future applications.

DW dynamics in ferromagnetic nanotubes have shown to be absent of those complex topological transformations, so analytical techniques are well situated to gain insight in the different DW regimes. In fact, the robustness of DW motion in MNTs combined with the intrinsic properties of the tubular geometry and the new advanced synthesis techniques [16–21], have fueled further investigations. Particularly, we find recent analytical and computational efforts focused to understand the properties of DWs in MNTs [22–31], among which we observe very suggestive properties from a technological point of view. This is the case of the chirality and

* Corresponding author. Tel.: +56 032 2654722.
E-mail address: jorge.otalora@usm.cl (J.A. Otálora).

0304-8853/$ - see front matter © 2013 Elsevier B.V. All rights reserved.
http://dx.doi.org/10.1016/j.jmmm.2013.04.014

propagation control of the vortex domain wall (VDW) by using constant and pulsed magnetic fields [29] and electric currents [30], which let us to envision possible applications related to the control of the VDW chirality as a new degree of freedom for storage devices. In order to avoid any further confusion with vortex domains walls in planar systems, we mention that the "vortex-like domain wall" studied here is quite similar to a transverse domain wall in a nanostripe, and can be obtained by unrolling the tube into a nanostripe [31]. On the other hand, with the exception of the very recent magnetoresistance measurements of Rüffer et al. [21], experimental work on this aspect has not been done yet, which could be seen as a good opportunity to open a new window for the design of devices based on the robustness of VDW dynamics in MNTs.

This paper is focused on revealing in-depth the properties of VDWs in MNTs. The high propagation speeds reached at weak applied magnetic fields and the breaking of chiral symmetry that gives origin to such chirality transformations constitute the main motivations of this research. It is demonstrated that a proper consideration of the dipole–dipole interaction and the tubular geometry explains: (i) the symmetry breaking, which is manifested by an additional dynamical instability (the *chiral breakdown*), and (ii) the DW propagation at high velocities for weak applied magnetic fields, which for permalloy nanotubes (of outer radius < 30 nm) range between 200–1000 m/s for field strengths between 0.7–1.0 mT [32]. We organize this paper as follows: in Section 2 we develop the theoretical model, in Section 3 we present our theoretical results and finally in Section 4 we outline the final remarks and conclusions.

2. Model

We consider a ferromagnetic nanotube confined in an ideal cylindrical shape with a perfect surface, so that pinning effects are not taken into account. We focus our attention on MNTs with large aspect ratio $L \gg R$, where L is the MNT length, while R and r correspond to the external and internal radii, respectively. In recent experiments, the authors synthesize MNTs with values of the order of R~15–300 nm, r/R~0.6–0.95, and L~1–20 μm [17,18]. Recent theoretical results show that the VDW is the most probable reversal mode, provided the external radius satisfies the relation $R > R_c(r/R, l)$, whereas for $R < R_c$ the reversal mode corresponds to a transverse DW [23]. Here, $l = \sqrt{2A/\mu_0 M_s^2}$ is the exchange length of the ferromagnetic material. Higher values of R_c are obtained for lower values of r/R, where $r/R = 0$ corresponds to a solid cylinder. So, according to the experimental values mentioned above, we only consider external radius limited by $R > 2l$ when $r \geq 0.6R$, in order to ensure a VDW as the energetically probable reversal mode. VDWs in MNTs consist of two regions of opposite magnetization parallel to the axis and separated by an intermedium zone (the DW). In that zone, the magnetization is in a vortex configuration almost tangential to the cylindrical mantle, but with a not necessarily zero radial component [27]. We observe four types of VDWs: two head-to-head (h2h) and two tail-to-tail (t2t), each one with two possible chiral states, clockwise (CW) and counterclockwise (CCW), as depicted in Fig. 1.

We follow a dissipative Lagrangian formalism to describe the VDW dynamics, which is based on the method of collective coordinates [27,33]. In this scheme, a VDW can be parameterized by three collective coordinates: (i) the DW center (z_0), (ii) the width (w), and (iii) the out-of-plane angle (p) which is a measure of the radial component of the magnetization (see Fig. 1). This magnetization model describes a h2h–VDW which is enough for the purposes of this paper. However, the extension of the model and subsequent results to a t2t–VDW are straightforward. For the normalized magnetization, $\vec{m} = \vec{M}/M_s$, expressed in terms of polar angles Θ and Ψ as $\vec{m} = (\cos\Psi \sin\Theta, \sin\Psi \sin\Theta, \cos\Theta)$, the model reads as

$$\Theta(z) = \begin{cases} \pi, & z > z_0 + \dfrac{w}{2} \\ \pi\left(\dfrac{z - z_0}{w} + \dfrac{1}{2}\right), & z_0 - \dfrac{w}{2} < z < z_0 + \dfrac{w}{2} \\ 0, & z < z_0 - \dfrac{w}{2} \end{cases} \tag{1}$$

$$\Psi(z) = \pi/2 - p. \tag{2}$$

In terms of the above magnetization model, the magnetic energy has been calculated for long tubes [27], which is given as

$$E = \frac{\pi A}{l^2} \int_0^\infty \left(\frac{\pi R}{wk} f_1(k) - k G_1(k) \sin p\right)^2 Q(k)\, dk \tag{3}$$

$$+ \pi^2 \frac{sA}{w} + \pi A \log\left(\frac{R}{r}\right) w - \frac{4sA}{l^2} \frac{H}{M} z_0, \tag{4}$$

where $s \equiv \pi(R^2 - r^2)$ is the tube cross-section, A is the exchange constant, and $f_1(k)$, $G_1(k)$ and $Q(k)$ are functions given in Appendix of Ref. [27] by Eqs. (A4), (A6) and (A9), respectively. The first term of the total energy (Eq. (3)) corresponds to the dipolar energy, the second and third terms give the exchange energy, and the last term corresponds to the Zeeman energy. It is worth noting that we focus our attention on MNTs with $r/R \geq 0.6$ in order to set the real system closer to our model, wherein the magnetization is independent of the radial coordinate. With this assumption, we safely discard the formation of Bloch points [22].

Following the Lagrangian formalism [27], it is found that the wall width is a slave coordinate, since its relaxation time is much

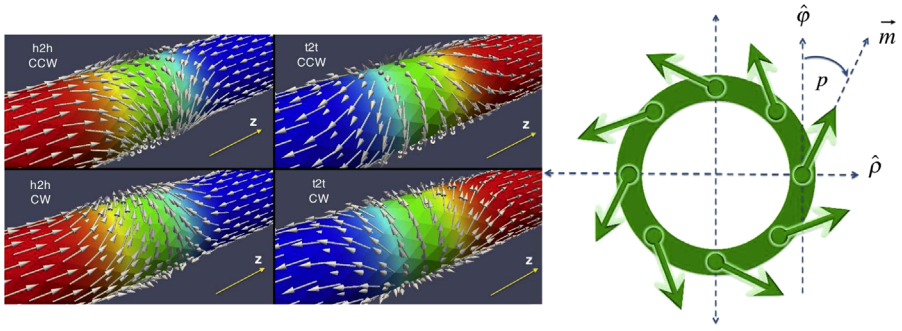

Fig. 1. Left panel: The four types of vortex domain walls in ferromagnetic nanotubes are shown. On the left panel we show a head-to-head (h2h) wall with a counterclockwise (CCW) and a clockwise (CW) chirality, and the same can be seen on the right panel for the tail-to-tail (t2t) wall. Right panel: Illustration of the magnetization component ($\vec{m}$) in the cross-section of the MNT at the center of the vortex wall. The angle p is a measure of the radial component of the magnetization and plays a key role in the dynamics of vortex domain walls.

faster than the other collective coordinates. This means that w depends on the instantaneous values of z_0 and p, and therefore the equations of motion for the remaining collective coordinates can be written as follows:

$$\dot{p}-\frac{\alpha\pi^2}{2}\frac{\dot{z}_0}{w}=-\frac{2}{\tau}h, \tag{5}$$

$$\dot{z}_0+\frac{\alpha w}{4}\dot{p}=-\frac{l}{\tau}\frac{\delta\varepsilon}{\delta p}, \tag{6}$$

where $h=H/M_s$, $\varepsilon=E/(\mu_0 M_s^2 ls)$, $\tau\equiv 2/(\gamma\mu_0 M_s)$, γ is the gyromagnetic ratio and $\dot{x}=dx/dt$ with $x=z_0$, p. The set of Eqs. (5)–(6) express the dynamics of a VDW through its collective coordinates (z_0, p, w). We write Eqs. (5) and (6) in a more convenient way

$$\dot{p}=-\frac{2}{\tau}\left[1+\frac{\pi^2\alpha^2}{8}\right]^{-1}(h+\alpha h_\rho(p)), \tag{7}$$

$$\frac{\dot{z}_0}{w(p)}=\frac{\alpha}{2\tau}\left[1+\frac{\pi^2\alpha^2}{8}\right]^{-1}\left(h-\frac{8}{\pi^2\alpha}h_\rho(p)\right). \tag{8}$$

Here, based in the similarity between the term

$$h_\rho(p)\equiv\frac{\pi^2 l}{4w(p)}\frac{\partial\varepsilon}{\partial p} \tag{9}$$

and the component in the $\hat{\Psi}$ direction of the effective field ($H_\Psi\propto\partial\varepsilon/\partial p$), it is possible to associate h_ρ to an effective-like field, which depends of the magnetic energy density of the material. As we see later, this field is responsible for the radial component of the vortex magnetization and the breaking of chiral symmetry mentioned above. We remark that this field is a helpful quantity, which provides a better understanding of the DW dynamics. Now, we proceed to discuss the global dynamical features of the VDW.

3. Results and discussion

In this section we discuss the VDW static properties, as well as its dynamical properties under the influence of an applied magnetic field. We emphasize the origins of breaking of chiral symmetry of DW propagation, and the motion at low applied fields, wherein its response to pulsed fields will be analyzed considering a particle-like description.

3.1. Vortex domain walls at zero applied field

The breaking of chiral symmetry of DW propagation and the small radial component at zero applied magnetic field are linked to each other. This can be understood in terms of the magnetic charges originating in the DW region. Those magnetic charges are the source of the magnetostatic energy and its corresponding volumetric density for a VDW reads

$$\sigma_V=-\vec{\nabla}\cdot\vec{M}=-\left(\frac{M_\rho}{\rho}+\frac{\partial M_z}{\partial z}\right). \tag{10}$$

For a h2h wall it is easy to note that $\partial M_z/\partial z<0$, which induces a preferential orientation of the radial magnetization. At zero applied field, the VDW tries to configure itself in order to reduce the volumetric magnetic charges, and hence, minimize the dipolar energy. So, in order to avoid magnetic poles, the magnetic moments acquire a radial component that points outward ($M_\rho>0$) from the external surface. On the other hand, surface charges on the MNT mantle appear with a non-zero radial magnetization, increasing the surface dipolar energy. Therefore, in order to reduce the total dipolar energy, the volumetric and surface contributions have to balance each other in such a way that the radial magnetization is restricted to small values [31].

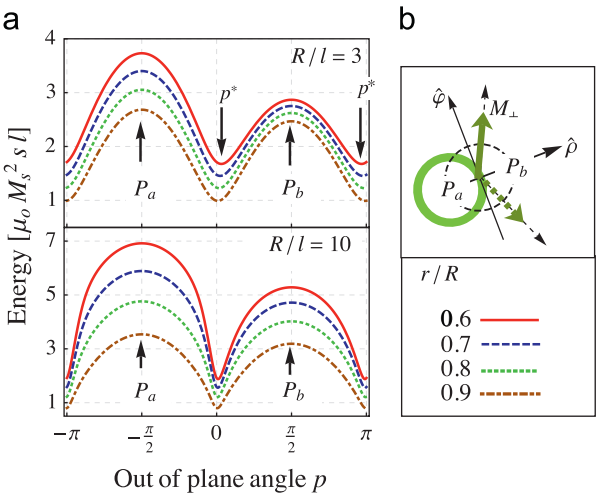

Fig. 2. (a) Total energy at zero applied field for a head-to-head vortex domain wall as a function of the out-of-plane angle p, for different outer and inner radii; and (b) illustration of the evolution paths P_a and P_b of the VDW radial component and its associated energy barriers.

A small radial magnetization component at the VDW region and other related properties are perceived from Fig. 2, wherein the total energy is plotted as a function of the radial angle p for $R/l=$ 3 and 10, and $r/R=0.6$, 0.7, 0.8 and 0.9. Here, we denote with p^* the out-of-plane equilibrium angle which minimizes the total energy. So, in consequence of the two possible DW chiralities, the total energy has two minima located at $p^*\approx 0$ for the CCW and at $p^*\approx\pi$ for the CW (see Fig. 2a). That the energy minimum is $p^*\gtrsim 0$ is linked with the localization of the global (local) energy maximum at $p=-\pi/2$ ($p=\pi/2$). In Fig. 2a those maxima are denoted by P_a and P_b, which label the energy barriers that the VDW has to overcome if the radial component evolves by twists around path P_a or path P_b, as illustrated in Fig. 2b. It is clear that twisting the radial magnetization through path P_a is more energetically expensive than twisting it around P_b. Indeed, the energy difference between these twisting paths is the origin of the chiral symmetry breaking, which as we will see in the next section, can be observed once a non-zero magnetic field is applied.

Another remarkable feature of the zero-field energy landscape is the limit of thinner tubes (when $r\to R$). Thinner tubes mean less volumetric charges, which in turn reduces the radial component of the magnetization and then the associated surface charges. In consequence, by the balance between the volumetric and surface dipolar energies, the equilibrium angle p^* increasingly approaches 0 (π) for CCW (CW) chirality, and the energy barriers located at $\pm\pi/2$ get equally closer each other. These tendencies are shown in Fig. 2a, wherein the thinner tube corresponds to $r/R=0.9$. In the limit of a very thin tube ($r\approx R$), the volumetric charges can be neglected and the dipolar contribution can be safely approximated with a surface anisotropy term, allowing the total energy to behave proportional to $\sin^2 p$ [27]. So, in a very thin tube where the equilibrium angles are 0 and π, the size of both energy barriers become equal each other, and the breaking of chiral symmetry disappears.

Formally, we describe the VDW properties at zero applied field through a set of dynamic equations (see (7) and (8)). In this case, we have to set $H=0$, $\dot{p}=0$ and $\dot{z}_0=0$ in order to determine the static properties, mainly featured by the equilibrium angles p^*. From Eqs. (7) and (8), these settings are equivalent to solve $h_\rho=0$. Then, the effective-like field h_ρ offers us information about: (i) p^* provided $h_\rho(p^*)=0$ and $\partial_p h_\rho(p^*)>0$, and (ii) the critical fields, given by the extremes of h_ρ (the inflection points in the energy).

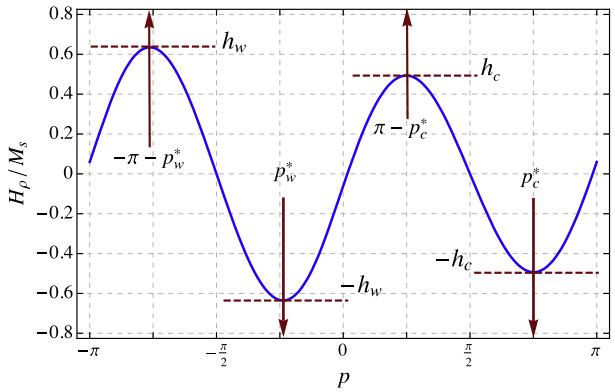

Fig. 3. Effective-like field of a head to head DW, as a function of the angle p for $R/l=3$ and $\beta=0.8$. The normalized critical fields h_w and h_c are related to the Walker field, and the chiral field at which the DW changes its chirality from CW to CCW. The angles p_w and p_c occurs at the onset of the Walker breakdown, and DW chirality transformation, respectively.

The general structure of the effective-like field shown in Fig. 3 is composed of the following characteristics: (i) four roots, two of them corresponding to the out-of-plane equilibrium angles, and the other two located at the magnetic energy maxima (at $p=\pm\pi/2$), and (ii) four extremes, a local (global) minimum at the angle p_c (p_w) closer to $p=3\pi/4$ ($p=-\pi/4$), and a local (global) maximum at the angle $\pi-p_c$ ($-\pi-p_w$) closer to $p=\pi/4$ ($p=-3\pi/4$) (see Fig. 3). We identify p_c and p_w as critical angles whose meanings are as follows: the critical angle p_c occurs at the onset of the DW chirality transformation, and the critical angle p_w occurs at the onset of the precessional motion at the Walker breakdown, as we see later. We denote the local (global) extreme magnitude by h_c (h_w), which is a very useful quantity to study the dynamical regimes of the VDW, and as we will see in the next section, p_c and h_c are two quantities that define the features of the breaking of chiral symmetry of DW propagations.

We note that the set of dynamic equations of the VDW in MNTs becomes quite similar to the equations of motion for a transverse DW in nanostripes, but just in the case that the dipolar energy is not so important and can be approximated by an effective anisotropy term. In this case, if we consider the limit of very thin nanotubes, it is easy to show that h_ρ~sin(2p) [12,27].

3.2. Dynamics of vortex domain walls driven by an homogeneous applied field

We now consider an external homogeneous magnetic field applied parallel to the tube axis. In this case, h2h–VDWs propagate in the same direction of the applied field, whereas t2t–VDWs move in the opposite direction. Usually, the applied field strength defines the following DW dynamical regimes: a steady motion (S) and a precessional motion (P). The details of each regime and the critical fields involved are analyzed solving the dynamic equations (7) and (8). Regarding the initial conditions, we assume that the VDW starts to move from rest where the initial state is determined by the out-of-plane equilibrium angle p^*. As we have seen above, a VDW begins with one of the two possible chiral configurations at the onset of the motion; CCW when p^* is close to 0, or CW when p^* is close to π. So, starting from these states, we solve the dynamic equations for a range of applied fields in order to allow the VDW to evolve through the different dynamical regimes, as shown in Fig. 4. Here, (a–d) shows the time evolution of the DW displacement (over the MNT axis) in the steady (S) and precessional (P) regimes, when the DW is under the action of applied fields of different magnitudes as illustrated by the different lines. Fig. 4(e, f) shows the applied field dependence of the average velocity and the corresponding equilibrium angle p^* for both initial chiralities (CCW and CW).

The appropriated range of applied magnetic fields can be defined with the aid of the parameters h_c and h_w, which (as discussed above) correspond to the extremes of the effective like-field h_ρ. We can associate the meaning of critical magnetic fields to these parameters as follows: (i) the well-known *Walker breakdown field* $H_w \equiv \alpha M_s h_w$, and (ii) a new dynamical instability called as the *chiral breakdown field* $H_c \equiv \alpha M_s h_c$. We note that $H_c < H_w$ because by definition $h_c < h_w$.

The steady motion of DWs in nanostripes is a well-known dynamical process in which, after a short transient time, the wall propagates with a constant velocity and a final configuration very close to the initial one [12]. However if we deal with VDWs in MNTs, we have to consider a new bound. Here, the steady motion splits into two ranges: (i) when $0<H<H_c$ and (ii) when $H_c<H<H_w$. In the first range, a VDW evolves during a transient stage from the initial configuration characterized by p^* (close to 0 for CCW and close to π for CW), until reaching the steady regime where the final state is defined by another equilibrium angle $p^*(H)$ which satisfies the condition $\dot{p}=0$ or $h_\rho(p^*)=-H/(\alpha M_s)$, and depends on the applied field (see Fig. 4f). At this range of applied fields, VDWs do not have enough energy to overcome any of the two energy barriers (see Fig. 2a), and therefore the walls preserve the initial chirality and continue the motion with (i) a constant velocity, as shown by the slopes in Fig. 4(a, c) for applied fields of 1 and 3 mT, and (ii) a well defined equilibrium angle which depends on H (see Fig. 4f). Otherwise, when the applied field is in the second range $H_c<H<H_w$, the transient stage is characterized by a chiral transformation from the initial CW chirality to the CCW one, wherein the walls suffer a recoil in the tube-axis propagation (see Fig. 4a for applied fields of 5.5 and 6 mT). However, the initial configuration is preserved if the DW starts the motion with an initial CCW chirality (see Fig. 4b for applied fields of 5.5 and 6 mT). This chiral dependence of the DW motion during the transient stage essentially defines the breakdown of chiral symmetry in vortex domain wall propagation in nanotubes. Once the transient process finish, the VDW continues its motion in a steady regime with CCW chirality.

The chirality transformation can be understood by looking at the torque exerted by the external field over the in-plane magnetization. According to the Landau–Lifshitz–Gilbert equation, the torque related to the magnetic field forces the DW to evolve with $\dot{p}<0$ [27], which means that the initial CW chirality follows the less energetically expensive path P_b, instead of traveling on path P_a, that is the path followed by an initial CCW wall, also with $\dot{p}<0$ (see Fig. 2). So, when $H_c<H<H_w$, the chiral symmetry breaks down. Since the CW domain wall has enough energy to overcome only the local energy barrier, after the transient stage its equilibrium angle becomes equal to the one reached by the CCW wall (see Fig. 4f at $H=H_c$). In t2t–VDWs, the chiral transformations occur from CCW to CW.

In every steady regime, the final velocity of the VDW can be written as

$$\langle \dot{z}_0 \rangle = \frac{4w(p^*)}{\tau\pi^2\alpha}\frac{H}{M_s}, \tag{11}$$

which is an expression very close to that obtained for TDWs in nanostripes and nanowires [12]. We observe that the average velocity is sensitive to the initial chirality only in the range $H<H_c$ wherein the chirality is preserved during the evolution (see Fig. 4 (e, f)). Here, CCW–VDWs moves faster than CW–VDWs, which is evident if we consider that each chirality evolves by a different energetic path. According to the discussion above, the CW follows the less energetically expensive path P_b instead of traveling on path P_a which is the path followed by the CCW wall (see Fig. 2).

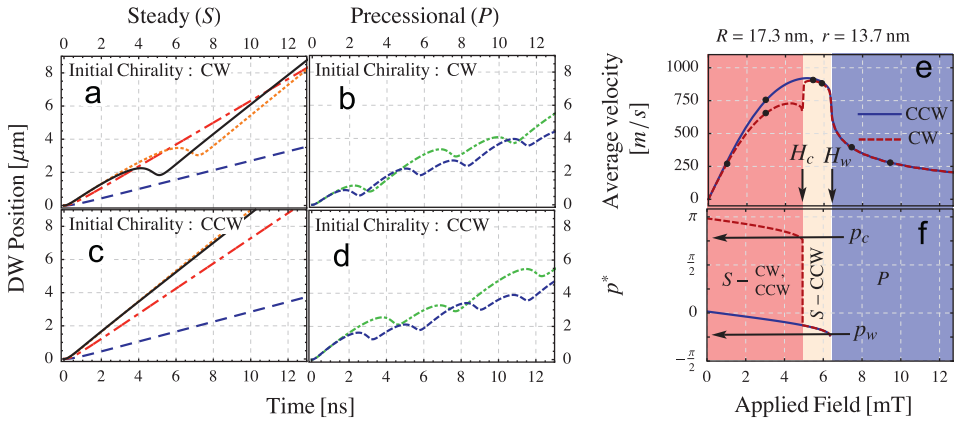

Fig. 4. (a–d) Time evolution of the position of the center of a h2h–VDW at the (a, c) steady (S) and (b, d) precessional (P) regimes for a Py MNT, which is initially configured as CCW and CW and is under the action of an applied magnetic field with different strengths. (a, c) The long-dashed, long-dashed dotted, dotted and full lines corresponds to fields amplitudes of 1, 3, 5.5 and 6 mT. (b, d) The dashed and dot-dashed lines are for 7.5 and 8.5 mT, respectively. Applied magnetic field dependence of the h2h–VDW average velocity and the associated equilibrium angle p^* are shown in (e) and (f) respectively. The dynamical regimes are represented by three shaded regions, which are defined by the chiral ($H_c \approx 4.9$ mT) and Walker ($H_w \approx 6.3$ mT) fields. The Gilbert damping parameter used is $\alpha = 0.01$.

Because of this, it can be demonstrated that the displacement of the CCW equilibrium angle is lower than the distance traced by the angle of the opposite chirality (the CW chiral state). As consequence the size of the CCW (CW) wall width is wider (narrower), and therefore, realizing that the average velocity is proportional to the VDW width, is straightforward to conclude that CCW chiralities will move faster than a vortex with CW chiral states (for the field configuration considered here). This velocity shift is another consequence of the chiral asymmetry in vortex domain wall propagation.

Otherwise, the VDW precessional regime occurs when the external field is greater than the Walker field ($H > H_w$). Here, the DW has enough energy to overcome both energy maxima, and hence, the out-of-plane angle (p) decreases continuously, running over all its possible values as time passes, because there is no equilibrium angle that satisfy the condition $h = -\alpha h_\rho(p^*)$. Consequently, the DW propagates undergoing precessions over the MNT axis, as demonstrated in Fig. 4(b, d). If a h2h–VDW starts precession with an initial CW chirality, the periodical motion will be composed by a short precession followed by a large precession; this order will be permuted for the case of the CCW. This behavior is consistent with the local and global energetic barriers of the energy landscape (see Fig. 2). Because of $\dot{p} < 0$ for a h2h–VDW, the CCW overcomes first the global and later the local barrier, showing a large and a short precession, respectively. On the contrary, the CW wall has to first climb with the local barrier and later the global one, letting the DW move with a short precession followed by the large one. As is well known, because of this precessional DW dynamics, the average velocity drops down (see Fig. 4a at $\mu_0 H > 6$ mT). This fact could be considered as a limitation from a technological standpoint if high velocities were required. To avoid the reduction in the average velocity, it might be possible to apply optimized time-dependent fields, following the method introduced by Tretiakov and Abanov [34]. These authors propose that the usage of time-dependent electric currents to drive a transverse DW in a nanostripe might reduce the Ohmic losses. They, additionally, found an optimized oscillation period for the time-dependent electric current, minimizing Ohmic losses. Furthermore they find that such oscillation period also avoids the reduction of the average velocity in the precessional regime. In our case the DW is driven by a magnetic field, so there is no Joule heating of the sample as in the case of current driven DW motion. However, the average velocity in the precessional regime can be increased applying time-dependent fields, with a period that depends on the geometry and magnetic field strength. Roughly speaking, from

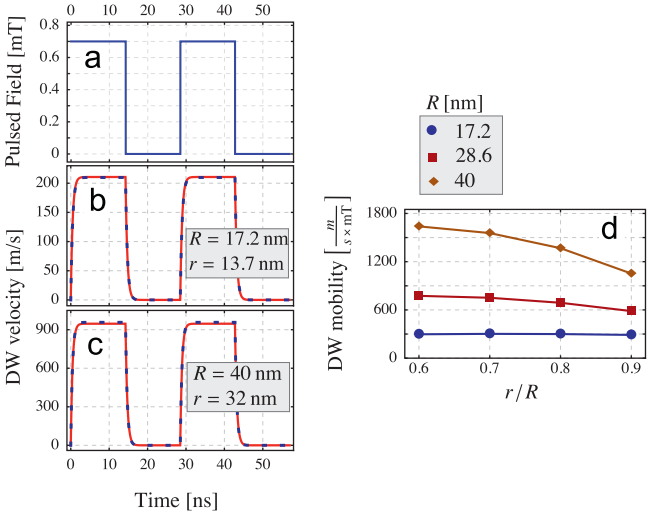

Fig. 5. (a) Pulsed magnetic field of weak amplitude (0.7 mT). (b, c) Velocity response of a head-to-head vortex domain wall under the application of the pulsed field on a permalloy MNT. The full (dashed) line corresponds to the analytical (linearized) approximation. (d) Domain wall mobility at low fields. The field pulse duration is $\Delta t = 1250\tau \approx 15$ ns and the relaxation time is $\tau_{rel} \approx 500\tau \approx 5.5$ ns.

Fig. 4(b, d) we can observe that the full period of DW precession (p from 0 to 2π) is about 6 ns for a field strength of 7.5 mT, and the maximum instantaneous speed occurs at about 1 ns. Then, if we apply a positive time-dependent field with a given profile, the full-width at half-maximum characterizing this profile should be of the order of 1 ns, in order to frustrate the precessional motion and, at the same time, increase the average velocity.

Finally, we note the linear behavior and high values of the average velocity at weak applied field strength around the millitesla orders. This is the case shown in Fig. 4(e) for a permalloy MNT in which VDWs reach velocities close to 300 m/s when $\mu_0 H = 1$ mT. It is worth to mention that these velocities increase considerably with the tube radius, as we will see in the next section (see Fig. 5d), where the dynamics in the low field regime is discussed.

3.3. Pulsed applied fields and low field regime

At weak applied fields ($H \ll H_w$), the VDW energy is close to a minimum, where $p^*(H) \approx p^*(H=0) \equiv p_0$. So, a linearization of the dynamic equations (7) and (8) around the initial chirality state,

allows us to understand the DW motion as a particle of mass $M_{DW}=(2sA\tau^2/l^3)(\partial^2\varepsilon/\partial p^2)^{-1}_{p_0}$ moving in a viscous medium, wherein the particle relaxes to reach the steady regime. The nature of this motion allows us to define a relaxation time $\tau_{rel}\equiv(2\tau w(p_0)/\ \alpha\pi^2 l)/(\partial^2\varepsilon/\partial p^2)_{p_0}$, as a typical time during which the wall tries to reach the steady regime with a terminal velocity $\overline{v}=\langle\dot{z}_0\rangle$. Then, the linearized dynamics is given as $\ddot{z}_0+(\dot{z}_0-\overline{v})/\tau_{rel}=0$ where $\overline{v}=\mu\mu_0 H$ and $\mu\equiv 2\gamma w(p_0)/(\pi^2\alpha)$ is the low-field mobility. For Permalloy with Gilbert damping $\alpha=0.01$ and most of the MNTs sizes that are experimentally achievable, our analytical model ranges the chiral and Walker fields between 3 mT and 7 mT (see Fig. 3 in Ref. [29]), $\tau_{rel}<500\tau\approx 6$ ns and $M_{DW}\sim 10^{-18}$–10^{-16} kg which is in agreement with the high mobility order $\sim 10^4\ \mathrm{T}^{-1}$ m/s.

Most of the DW properties at weak fields applied over several representative MNT sizes are summarized in Fig. 5. To know the reliability of the low field approximation, the DW motion is calculated by the full analytical equations (6) and (7), and by the linearized version when the applied field consists of pulses with low amplitude. Fig. 5(a–c) shows that pulses with 0.7 mT of amplitude let the VDW reach high velocities of propagation, around 200 m/s (900 m/s) for the smaller (bigger) permalloy nanotube. This is in agreement with the high values of the low-field DW mobility μ which is plotted in Fig. 5d. Here, the DW mobility increases with the outer radius and decreases with the thickness diminution. This property is better understood by recognizing two characteristics: (i) the mobility is proportional to the VDW width $w(p_0)$ and (ii) the wall width grows with nanotubes of larger outer radius and greater thickness. We also observe that the DW velocity tries to mimic the pulsed field shape with a good fidelity. In fact, the fidelity can be enhanced if the pulse duration Δt is conditioned to be much larger than the relaxation time ($\Delta t\gg\tau_{rel}$), which ranges around a few nanoseconds for most of the experimental MNT sizes [16–21].

Finally, we remark that a short relaxation time and a high DW velocity linked by a linear relation to a weak strength of the applied field, might be a set of required properties in order to obtain a reliable control of the DW motion with a fast response to external magnetic fields. According to our previous results, that is (high speed of propagations around 200 m/s (900 m/s), for the smaller (bigger) Py tube and 0.7 mT of pulse amplitude, and relaxation times around nanoseconds) we think that VDWs in MNT accomplish those features, which make these kinds of walls attractive from a technological standpoint.

4. Conclusions and final remarks

Dynamics of vortex domain walls (VDW) in long ($L\gg R$) magnetic nanotubes under the action of an external magnetic field have been investigated analytically. It has been shown that VDW dynamics depend strongly on the initial chirality, a direct consequence of the so-called *breaking of chiral symmetry in vortex domain wall propagation*. We have traced this breaking until the VDW energetic asymmetry, as shown by Fig. 2, wherein the two energy barriers of different sizes involve a more (less) expensive evolution path P_a (P_b) of the VDW out-of-plane angle p, which at the same time privileges the DW propagation of just one kind of chirality, and two critical fields, the well-known Walker breakdown field $H_w\equiv\alpha M_s h_w$ and the so-called *chiral field* $H_c\equiv\alpha M_s h_c$, wherein h_w (h_c) is the inflection point associated to the global (local) energy barrier. Accordingly, we have found that the VDW dynamics is divided in the two usual regimes: (i) the steady motion (see Fig. 4(a, c) for $H<H_w$), and (ii) the precessional motion (see Fig. 4(b, d) for $H>H_w$). However, as consequence of the chiral asymmetry of VDW propagations, the steady regime is affected by the chiral field H_c. When the external field is lower than the chiral field $H<H_c$, both initial VDW chiralities are retained during the motion, and just one of them undergoes faster propagation speeds (see Fig. 4e), and when $H_c<H<H_w$ just one of the initial chiralities is retained.

Finally, we investigated the VDW behavior at weak applied fields. We have found that the VDW relaxes during a typical time τ_{rel} until reaching the steady regime with a terminal velocity $\overline{v}=\mu H$, where μ is the low-field mobility. The high mobility values around $10^4\ \mathrm{T}^{-1}$ m/s (see Fig. 5d) and the short relaxation times around nanoseconds, allow VDWs to propagate at surprisingly high values of terminal velocities (around 200 m/s (900 m/s) for the smaller (bigger) Py nanotube) for a amplitude of 0.7 mT, and at the same time with a reliable control of the DW velocity if the external field amplitude is modulated (see Fig. 5(a–c)).

Acknowledgments

The authors acknowledge support from CONICYT, FONDECYT under Grants 3130457, 1110271, 1100508 and 1120618, PIIC-UTFSM 2012, "Proyecto Anillo de Ciencia y Tecnología" ACT 1117 and by the “Financiamiento Basal para Centros Científicos y Tecnológicos de Excelencia” CEDENNA FB0807.

References

[1] S.S.P. Parkin, M. Hayashi, L. Thomas, Science 320 (2008) 190.
[2] D. Atkinson, C.C. Faulkner, D.A. Allwood, R.P. Cowburn, Spin dynamics in confined magnetic structures III, in: B. Hillebrands, A. Thiaville (Eds.), Topics in Applied Physics, vol. 101, Springer-Verlag, Berlin, 2006, p. 207.
[3] T.J. Silva, W.H. Rippard, Journal of Magnetism and Magnetic Materials 320 (2008) 1260.
[4] S.A. Wolf, D.D. Awschalom, R.A. Buhrman, J.M. Daughton, S. von Molnár, M. L. Roukes, A.Y. Chtchelkanova, D.M. Treger, Science 294 (2001) 1488.
[5] A. Fert, Reviews of Modern Physics 80 (2008) 1517.
[6] D. Sellmyer, R. Skomski (Eds.), Advanced Magnetic Nanostructures, Springer, New York, 2006.
[7] N.L. Schryer, L.R. Walker, Journal of Applied Physics 45 (1974) 5406.
[8] R.D. McMichael, M.J. Donahue, IEEE Transactions on Magnetics 33 (1997) 4167.
[9] Y. Nakatani, A. Thiaville, J. Miltat, Nature Materials 2 (2003) 521.
[10] D.G. Porter, M.J. Donahue, Journal of Applied Physics 95 (2004) 11.
[11] G.S.D. Beach, C. Nistor, C. Knutson, M. Tsoi, J.L. Erskine, Nature Materials 4 (2005) 741.
[12] A. Thiaville, Y. Nakatani, in: B. Hillebrands, A. Thiaville (Eds.), Spin Dynamics in Confined Magnetic Structures III, Topics in Applied Physics, vol. 101, Springer-Verlag, Berlin, 2006, p. 161.
[13] D.J. Clarke, O.A. Tretiakov, G.W. Chern, Ya.B. Bazaliy, O. Tchernyshyov, Physical Review B 78 (2008) 134412.
[14] J-.Y. Lee, K-.S. Lee, S. Choi, K.Y. Guslienko, S-.K. Kim, Physical Review B 76 (2007) 184408.
[15] R. Wieser, E.Y. Vedmedenko, P. Weinberger, R. Wiesendanger, Physical Review B 82 (2010) 144430.
[16] Y.C. Sui, R. Skomski, K.D. Sorge, D.J. Sellmyer, Applied Physics Letters 84 (2004) 1525.
[17] K. Nielsch, F.J. Castaño, C.A. Ross, R. Krishnan, Journal of Applied Physics 98 (2005) 034318.
[18] J. Bachmann, J. Jing, M. Knez, S. Barth, H. Shen, S. Mathur, U. Gösele, K. Nielsch, Journal of the American Chemical Society 129 (2007) 9554.
[19] J. Escrig, M. Daub, P. Landeros, K. Nielsch, D. Altbir, Nanotechnology 18 (2007) 445706.
[20] Q. Wang, B. Geng, S. Wang, Y. Ye, B. Tao, Chemical Communications 46 (2010) 1899.
[21] D. Rüffer, R. Huber, P. Berberich, S. Albert, E. Russo-Averchi, M. Heiss, J. Arbiol, A. Fontcuberta i Morral, D. Grundler, Nanoscale 4 (2012) 4989.
[22] R. Hertel, J. Kirschner, Journal of Magnetism and Magnetic Materials 278 (2004) L291.
[23] P. Landeros, S. Allende, J. Escrig, E. Salcedo, D. Altbir, E.E. Vogel, Applied Physics Letters 90 (2007) 102501.
[24] J. Escrig, P. Landeros, D. Altbir, E.E. Vogel, Journal of Magnetism and Magnetic Materials 310 (2007) 2448.
[25] P. Landeros, O.J. Suarez, A. Cuchillo, P. Vargas, Physical Review B 79 (2009) 024404.
[26] A.P. Chen, K.Y. Guslienko, J. Gonzalez, Journal of Applied Physics 108 (2010) 083920.
[27] P. Landeros, A.S. Núñez, Journal of Applied Physics 108 (2010) 033917.
[28] J.A. López-López, D. Cortés-Ortuño, P. Landeros, Journal of Magnetism and Magnetic Materials 324 (2012) 2024.

[29] J.A. Otálora, J.A. López-López, P. Vargas, P. Landeros, Applied Physics Letters 100 (2012) 072407.
[30] J.A. Otálora, J.A. López-López, A.S. Núñez, P. Landeros, Journal of Physics: Condensed Matter 24 (2012) 436007.
[31] M. Yan, C. Andreas, A. Kákay, F. García-Sánchez, R. Hertel, Applied Physics Letters 99 (2011) 122505.
[32] For comparison, the usual maximum velocity reached by a DW in nanostripes ranges between 100–500 m/s at applied magnetic fields ranging between 5–20 mT [9,12,14].
[33] O.A. Tretiakov, D. Clarke, G-.W. Chern, Y.B. Bazaliy, O. Tchernyshyov, Physical Review Letters 100 (2008) 127204.
[34] O.A. Tretiakov, Y. Liu, Ar. Abanov, Physical Review Letters 105 (2010) 217203.